ADVANCED MATERIALS TECHNOLOGIES
www.advmattechnol.de

# 3D-Printed Anisotropic Nanofiber Composites with Gradual Mechanical Properties

*Florian Lackner, Ivan Knechtl, Maximilian Novak, Chandran Nagaraj, Andreja Dobaj Štiglic, Rupert Kargl, Andrea Olschewski, Karin Stana Kleinschek, and Tamilselvan Mohan**

**3D printing of bio-based nanomaterials into complex structures with design flexibility, structural anisotropy, and long-term stability is a key issue for biomedical applications. Herein, 3D-printed and ionically crosslinked structures with anisotropic, water-proof, and tunable mechanical properties are fabricated using a polysaccharide ink composed of nanocellulose, alginate, and $CaCO_3$ nanoparticles. The excellent shear thinning properties of the ink, combined with double or even triple extrusion, allow printing of complex structures (tubes, buckets, ears, and boat models) with high shape fidelity even after crosslinking. The anisotropically printed and crosslinked structures can be mechanically tuned by controlling the fiber orientation via the printing path, the amount of crosslinker, the type of acid used for crosslinking (weak to strong), and the storage medium. This allows for tailored flexibility and a tensile modulus of the materials in wet state ranging from 1 to 30 MPa. Application of hydrostatic pressure of 160–600 mmHg for 24 h with a physiological fluid to a tubular structure, a model for the cardiovascular system, shows no leakage or rupture in the tube. The great design freedom offered by 3D printing and spatially controlled structural anisotropy enable the production of tailored materials for soft robotics or biomedical applications.**

## 1. Introduction

Nature served as a source of inspiration for the creation of functional anisotropic materials, which exhibit different mechanical or physical properties in different directions due to heterogenous structures or compositional gradients.[1–3] For example, several biological tissues exhibit highly aligned or anisotropic structures of collagen fibers that provide them the required load-bearing capacity.[1,4] Inspired by this anisotropic structure, aligned reinforcements have been introduced into load-bearing materials to achieve the maximum possible mechanical performance in the required direction.[5] Bioinspired structure is commonly used in engineering to create anisotropic materials that provide directional enhancement of strength, swelling, or thermal properties and perform specific functions such as tunable shape recovery, polarized patterning, or fluid resistance.[4] These anisotropic materials have sparked long-term research interest in tissue engineering (TE) to mimic the mechanical strength of biological tissue. The strength and elasticity of soft biological tissues, including cardiac muscles, arteries, veins,[6,7] are in the range of 1–10 MPa tensile strength at break, and 1–30 MPa elastic modulus.[8,9] To date, various materials and methods have been investigated and developed with the ambition to replicate, or at least imitate the structural, mechanical, and functional features of biological tissue. This is done with the motivation to increase our basic understanding,[10,11] to influence cell growth in TE,[12] or to apply materials as medical phantoms.[13]

Direct-ink-writing (DIW) is a widely used extrusion-based 3D-printing method for the production of complex, customizable, and flexible structures used in TE, soft robotics, and others.[14–16] By precisely controlling the print pattern, pathway,

F. Lackner, I. Knechtl, M. Novak, R. Kargl, K. Stana Kleinschek, T. Mohan
Institute for Chemistry and Technology of Biobased System (IBioSys)
Graz University of Technology
Stremayrgasse 9, Graz 8010, Austria
E-mail: tamilselvan.mohan@tugraz.at

The ORCID identification number(s) for the author(s) of this article can be found under https://doi.org/10.1002/admt.202201708.



DOI: 10.1002/admt.202201708

C. Nagaraj, A. Olschewski
Ludwig Boltzmann Institute for Lung Vascular Research
Stiftingtalstrasse 24, Graz 8010, Austria

A. Dobaj Štiglic, R. Kargl, T. Mohan
Laboratory for Characterization and Processing of Polymers
Faculty of Mechanical Engineering
University of Maribor
Smetanova Ulica 17, Maribor 2000, Slovenia

A. Olschewski
Department of Anaesthesiology and Intensive Care Medicine
Medical University of Graz
Graz 8036, Austria

K. Stana Kleinschek
Institute of Automation
Faculty of Electrical Engineering and Computer Science
University of Maribor
Koroška cesta 46, Maribor 2000, Slovenia

 

and extrusion pressure, an unprecedented level of freedom in the design of self-standing structures, actuators, and programmable materials can be obtained.[17–20] Synthetic polymers such as flexible silicone-like resins have been used to 3D print medical anatomical models of blood vessels with stereolithography[21] whereas synthetic, solvent-free poly(n-butyl acrylate) elastomer brushes[6] or composites[22] are known to exhibit similar stress–strain curves as some soft biological tissue. Combining 3D printing with material science has therefore a significant potential in the field of tissue mimetics and TE.

Polysaccharides (glycosaminoglycans, proteoglycans), proteins (collagen, elastin), fats, and water are the inherent constituent of mammalian tissue, whereas cellulose is the load bearing component in plants and bacterial biofilms.[10,23,24] All constituents contribute to the biomechanical properties of living tissue and imitating tissue properties can benefit from understanding and using these bio-based materials.[25] Related to that, cellulose nanofibrils (NFC) have attracted considerable attention, and in some instances extrusion processes provide access to structural anisotropy leading to remarkable mechanical properties.[15,26] NFC has as high strength-to-weight ratio[27] and could be regarded as a type of plant-based collagen with respect to its mechanical function in cells.[28,29] It is therefore of interest to investigate the (bio-)mechanical properties of anisotropic and 3D-printed NFC and compare it with mammalian vascular tissue.

Since NFC cannot be printed into stable shapes without crosslinking, at least one matrix component is needed that imitates the extracellular or cell wall polysaccharides which surround the load-bearing fibers in tissue. An example is alginate (Alg), which is found in the cell walls of algae[10,30] and known to contribute to the strength and flexibility of the plant by surrounding cellulose fibrils and by interacting with ions and water.[31] NFC and Alg are considered xeno-free and U.S. Food and Drug Administration-compliant materials[32] and have consequently been used to develop inks for DIW.[33–35] Alg can be crosslinked by post-printing with divalent ions forming "egg-box" structures.[16,20,32,36,37] $CaCl_2$ crosslinking after DIW can lead however to loss of shape fidelity, extensive swelling, and structural collapse.[38] Alternatively, water insoluble $CaCO_3$ (nano) particles can be incorporated into the ink and then solubilized by weak acids such as gluconolactone (Gdl).[39,40] The gradual dissolution leads to a progressive release of $Ca^{2+}$, enabling uniform crosslinking.[41,42] This crosslinking approach, especially in sterile medium such as ethanol (EtOH), is to our knowledge not used for DIW 3D-printed materials and is investigated here.

Inks from NFC/Alg/$CaCO_3$ for DIW are formulated and anisotropic, water stable and structures with spatially controlled mechanical properties are 3D printed during which fibers align. The influence of i) fiber orientation, ii) crosslinking media, iii) sample storage, iv) $CaCO_3$ concentration, and v) calcium leaching on the mechanical properties in the wet state is investigated and compared with biological tissue. Infrared spectroscopy and $CO_2$ release measurements are performed to follow the crosslinking kinetics, while scanning electron and optical microscopy is used to study calcium distribution and nanofiber alignment in the prints. The versatility of the method and materials is shown by manufacturing twistable stable shapes, with structural, swelling and mechanical anisotropy/gradients. The materials can potentially be used to imitate vascular tissue in terms of tensile strength and elongation at brake, biological fluid resistance, and biocompatibility. More complex shapes can be constructed including for TE as demonstrated with printed tubes capable of withstanding a pressure up to 600 mg Hg under physiological conditions.

## 2. Results and Discussion

### 2.1. Nanocomposite Ink Preparation and 3D Printing

The process of ink preparation, printing alignment, crosslinking, and analysis is shown in **Figure 1**. Homogeneity, high viscosity, and shear thinning are essential ink properties for a reliable and reproducible DIW process. A three-component ink (see **Table 1**) consisting of NFC (length: several micrometers, width: ≈20 nm, COONa: 0.35 ± 0.05 mmol $g^{-1}$),[27] Alg (2.63 ± 0.12 mmol $g^{-1}$, see Figure S1, Supporting Information), and $CaCO_3$ (69 ± 1 nm)[43] were directly mixed in the 3D-printing tube. To avoid prior dissolution steps, a straightforward two-step mixing process was used. First, the $CaCO_3$ was dispersed in the less viscous NFC suspension (3 wt% solids). The strong shear thinning properties of NFC (see Figure S2a, Supporting Information) are advantageous for initially dispersing the $CaCO_3$ particles at high shear rates, which prevented the particles from sedimentation and agglomeration before the stepwise addition of Alg. To address the problem of undissolved/dispersed components sticking to the walls and to minimize material loss due to transfer into the mixing vessel, a 3D-printed stirrer (see Figures S2d and S3d, right, Supporting Information) was developed to fit into the printing tube. This stirrer minimized dead mixing zones and material loss and enabled the production of a homogenous inks within ≈10 min. It also prevented clogging of the 260 and 410 µm diameter printing nozzles used to extrude the ink and delivered superior results compared to inks produced differently (Figures S2 and S3, Supporting Information). The homogeneity of the ink was assessed by light microscopy (Figures S2a–c and S5, Supporting Information), which qualitatively showed a uniform distribution of $CaCO_3$ and NFC, except some visible air bubbles.

A smooth flow through the fine nozzles during DIW is important, while maintaining a sufficiently high yield stress and storage modulus ($G'$) to maintain filament shape fidelity during printing.[15] The rheological results (Figure S2a, Supporting Information) showed that inks containing all three components are shear thinning with viscosity flow curves similar to the curve of neat NFC. This may be due to increased interfacial adhesion between NFC and Alg,[10,27] which favors the rheological behavior and thus excellent printability (see Figure S2f, inset, Supporting Information). Only minor differences were observed between the viscosity of the inks prepared with different concentrations of $CaCO_3$, which can be due to the relatively low amounts added. Figure S1b–d in the Supporting Information shows that all three-component inks behaved similarly to a rheological gel or a soft solid with high elastic gel strength, as reflected by a higher storage modulus $G'$ and a lower loss factor (tan $\delta$, $G''/G' < 1$).[11,34] The storage moduli increased with the addition of $CaCO_3$. An explanation can be that the interaction between NFC and ALG is enhanced

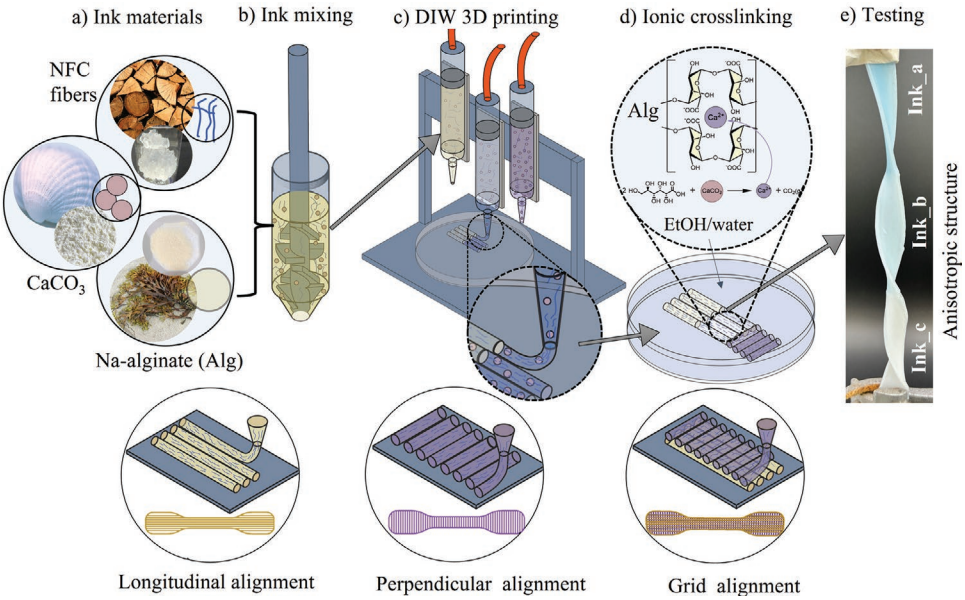


**Figure 1.** Schematic process overview of multiextrusion DIW 3D printing: a) materials required for ink preparation comprising NFC from wood pulp, $CaCO_3$ NPs, and Alg from brown algae, b) mixing process using a tailor-made stirrer directly in the printing tube, c) printing a scaffold with different ink compositions and fiber alignments, d) crosslinking with Gdl to release free $Ca^{2+}$ to form the "egg-box" structure, and e) material testing of the flexible objects exhibiting anisotropic structures.

by minor amounts of released calcium ions and particles adsorbed to the fibers.

We also investigated the printability of the inks and the shape fidelity of the printed structures before and after crosslinking with $Ca^{2+}$ in different environments. This is very important to ensure the quality and stability of the crosslinked structures for further characterization and processing. This aspect is still poorly addressed in the literature. Figure S2e,f in the Supporting Information shows the optical microscopic images and calculated strand distance (pores) of different layers printed with Inks (Ink**0.1**–Ink**1.1**) containing increasing concentrations of $CaCO_3$. As expected, the distance between printed strands decreased with increasing number of layers. This effect was observed for all inks but was more pronounced for the Ink with the highest $CaCO_3$ concentration (Ink**1.1**). The latter also showed nicely printed lines and excellent shape fidelity (Figure S2e, inset, Supporting Information), which had a larger storage modulus.

### 2.2. Crosslinking and Structure Stabilization

Since 3D printing requires a lot of effort to produce defined, ready-to-use shapes, the shape fidelity and dimensional stability of the printed objects after crosslinking plays a crucial role. Different crosslinking approaches were therefore investigated to find the right conditions under which the shape fidelity of printed cubic structures ($12 \times 12 \times 7$ mm$^3$, ≈1 mL) can be retained. Crosslinking was performed using Gdl, $CaCl_2$, and HCl dissolved in EtOH/$H_2O$ (50/50 wt%) or in water. In Gdl/$H_2O$ system, a strong swelling to more than 80 vol% of the crosslinked scaffold or even partial destructing was observed (**Figure 2**a). This was noticed for all crosslinking systems.[42] Crosslinking with HCl as a strong acid in water resulted in a change of shape from cubic to spherical, suggesting that HCl acts similarly to a foaming agent. The same results were obtained for the structures crosslinked with $CaCl_2$ in water. Gdl dissolved in ethanol/water led to excellent shape retention with a length shrinkage of 1.1 ± 0.2%. When crosslinking was performed with either HCl or $CaCl_2$ in ethanol/water, the shape fidelity of the crosslinked structure was better, especially with $CaCl_2$. However, the final structure shrank up to nine times more (9.9 ± 0.5%) compared to the Gdl system. Obviously, the shape fidelity and dimensional stability were considerably far better when crosslinked with Gdl in EtOH/$H_2O$ compared to water alone. The ethanol stabilizes the scaffold by dehydration in the initial phase until the weak glucuronic acid slowly releases the $Ca^{2+}$.[44] This slow release, especially from the formed $CO_2$, is important to maintain the printed structural stabilization and fidelity for further characterization and processing.

To observe the differences in $CO_2$ release kinetics during crosslinking with Gdl and HCl in EtOH/$H_2O$ for the first time, the $CO_2$ concentration was monitored using a 3D-printed home-built temperature-controlled measurement cell (see Figure S4, Supporting Information) with two different sample geometries (see Figure 2b). While the $CO_2$ concentration was

**Table 1.** Preparation of nanocomposite inks for DIW 3D printing.

| Inks | NFC | | Alg | | $CaCO_3$ NPs | |
|---|---|---|---|---|---|---|
| | [g] | wt% | [g] | wt% | [g] | wt% |
| Ink**0.1** | 20 | 2.8 | 1.33 | 6.2 | 0.061 | 0.1 |
| Ink**0.3** | 20 | 2.8 | 1.33 | 6.2 | 0.121 | 0.3 |
| Ink**1.1** | 20 | 2.8 | 1.33 | 6.2 | 0.363 | 1.1 |

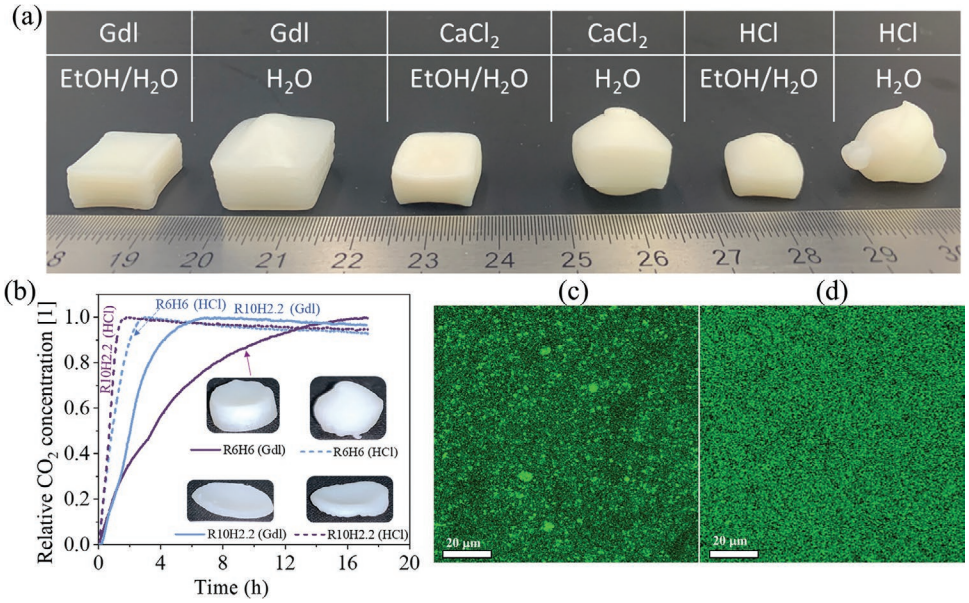


**Figure 2.** a) 3D printed cube (12 × 12 × 7 mm$^3$, ≈1 mL) from Ink**1.1** and crosslinked using Gdl, $CaCl_2$, HCl in EtOH/$H_2O$ and $H_2O$, b) release of $CO_2$ measured during crosslinking by Gdl and HCl at ambient condition; inset shows two different sample sizes used for crosslinking, and SEM-EDX mapping of calcium in the printed dried cube c) before and d) after crosslinking using Gdl in EtOH/$H_2O$.

saturated after 3 h when HCl was used, regardless of sample size (see inset, Figure 2b), the release with Gdl was slower and took up to 6 h or even 16 h to saturate with the more voluminous scaffold with longer diffusion path. As mentioned above, the weak glucuronic acid (p$K_a$ 3.6) provides less hydronium ions upon dissolution compared to the strong HCl (p$K_a$ −5.9), resulting in a slower release of $CO_2$ by dissolving $CaCO_3$.[44,45] It is obvious that the combination of $CaCO_3$/Gdl and EtOH/$H_2O$ is highly beneficial to achieve uniform crosslinking and thus maintain shape fidelity of the printed structures.

The presence and the distribution of $CaCO_3$ or calcium in the 3D printed structure before and after crosslinking was investigated by optical microscopy (Figure S5a–d, Supporting Information) and scanning electron microscopy-energy dispersive X-ray (SEM-EDX) mapping (Figure 2c,d). Optical microscopy (bright and dark-field modes) shows the even distribution of $CaCO_3$ particles throughout the noncrosslinked sample. SEM-EDX mapping (Figure 2c) showed a strong and bright signal for calcium evenly distributed in the matrix with particle diameters less than 12 µm. The presence of $CaCO_3$ particles could not be detected in the crosslinked sample, as shown by the optical microscope image. In the case of SEM-EDX (Figure 2d), there was a less bright signal but a more uniform calcium distribution. To further confirm this, we performed an IR analysis for air-dried samples (see Figure S6, Supporting Information). The latter showed the presence of carbonate peaks at 1460 and 874 cm$^{-1}$ stemming from $CaCO_3$ for the noncrosslinked samples,[43,46] while no such peak was observed for the crosslinked ones. All these results clearly indicate that the $CaCO_3$ was dissolved or hydrolyzed by glucuronic acid and turned into calcium ions, which are essential to achieve uniform crosslinking and structural stabilization.

### 2.3. Mechanical Properties

The materials exhibiting mechanical, structural, or swelling anisotropy are highly interesting, as phantoms, to mimic or to replace the natural tissue.[4] The introduction and control of these properties in the NFC/Alg nanocomposites is a great challenge and has not been described before. Here, we specifically investigated the influence of four different conditions on the wet tensile properties (along with structure and swelling) of 3D-printed NFC/Alg specimens: i) fiber orientation, ii) crosslinking agent, iii) storage and application solution, and iv) concentrations of $CaCO_3$ in the ink. These four different conditions can be independently combined to create anisotropic NFC/Alg biostructures for the desired application.

#### *2.3.1. Effect of Fiber Orientation*

The high aspect ratio of the NFC and the shear forces created by forcing the ink through the small nozzle allow the fibers to be aligned along the axis of the printed direction.[47] This has a significant effect on the mechanical and swelling properties of printed specimens, which was addressed in this work by 3D-printing sheets with different strand placement directions. The samples in dumbbell-shape to match the intended fiber direction, specimens with fiber orientation: longitudinal, perpendicular, or grid (a combination of both) to the test direction was punched-out, crosslinked using Gdl in EtOH/$H_2O$ medium and tested (condition i, see **Figure 3**a,b). We used cast and crosslinked samples in the same way as above for comparison. Figure 3a,b compares the stress–strain curves and mechanical properties of cast and 3D-printed specimens after crosslinking. All specimens showed a monotonous increase in stress until

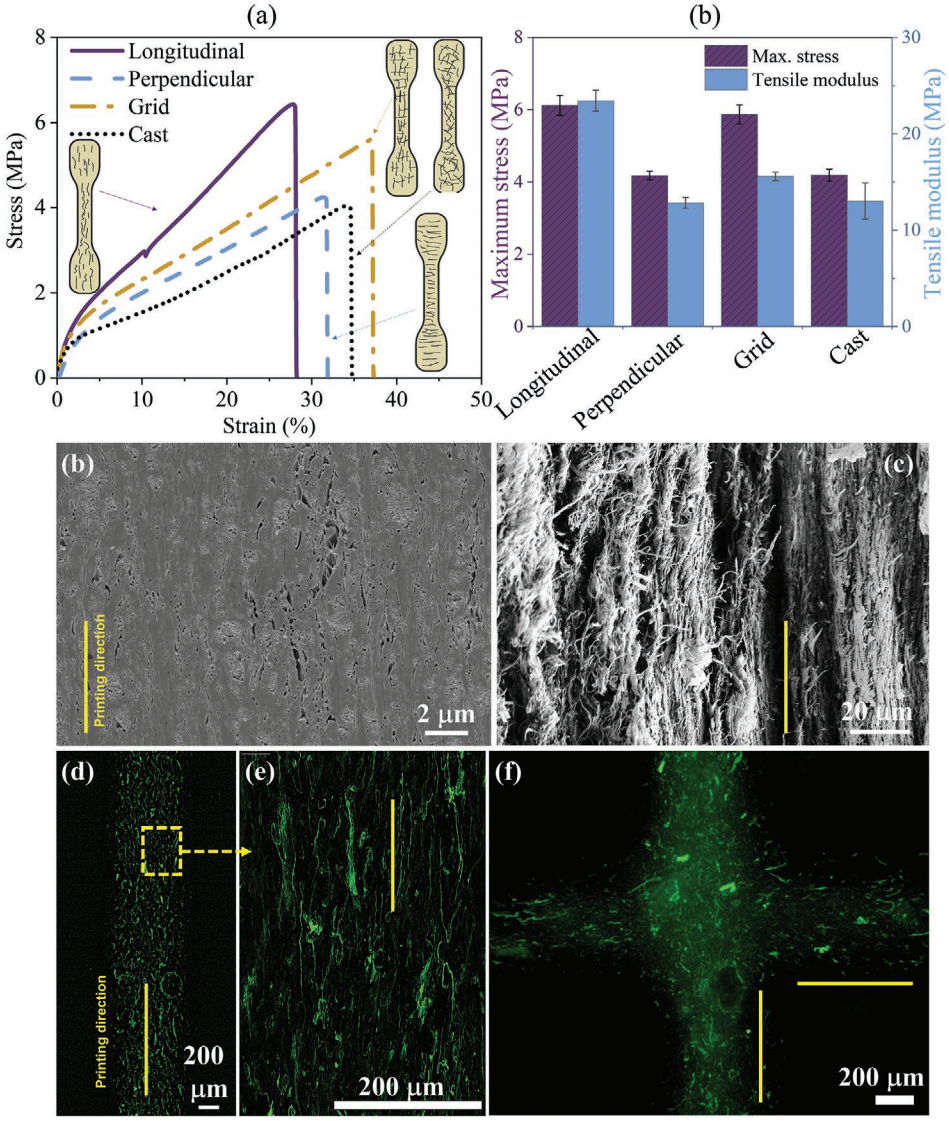


**Figure 3.** Mechanical properties, microscopic images of the NFC/Alg structures, crosslinked structures using Gdl in EtOH/$H_2O$. a) Tensile stress–strain curves and b) comparison of mechanical properties of structures printed from Ink**1.1** at different directions (fiber orientation) and crosslinked; cast sheet from Ink**1.1** used for comparison. SEM images (b: surface and c: cross-section) of crosslinked NFC/Alg structures (air-dried). d–f) Fluorescence microscope images of longitudinally (d: surface and c: cross-section) and grid printed and crosslinked structures. The printing direction (fiber alignment) is indicated by a solid yellow line in both SEM and fluorescence images.

fracture.[48,49] The latter is a characteristic feature of nanocellulose/alginate-based materials resulting from the deformation-induced reorganization (straightening and alignment) of the NFC or Alg network in the structure.[47,49] Samples pulled uniaxially to the fiber direction (longitudinal) appeared to be twice as strong, with a modulus of 23.4 ± 1.1 MPa compared to 12.8 ± 0.6 MPa for the perpendicular case. The observed tensile stress (4.2 ± 0.1 MPa) was also 25% lower for the latter sample. Cast specimen with an assumed random fiber orientation showed similar results to fibers oriented perpendicular to the test direction, with a stress and modulus of 4.2 ± 0.2 and 13.0 ± 1.5 MPa. The grid with alternating orientation patterns in each layer with longitudinal and perpendicular orientation showed a tensile modulus of 15.6 ± 0.4 MPa and tensile modulus similar to that of longitudinal case when the two orientation effects are averaged. This nearly twofold difference in tensile modulus allows further tailoring of the mechanical properties of the printed scaffolds by directing the print path to achieve the desired orientation. Not only tensile modulus, but also electrical,[50] optical,[51] biological,[52] and swelling properties could be affected by shear force-induced fiber alignment during 3D printing of hydrogel composites.

Fiber alignment in the Gdl-crosslinked structures was confirmed by SEM (Figure 3b,c, showing longitudinally printed structures) and fluorescence (Figure 3d–f, showing longitudinally and grid printed structures) microscopic analysis. For the latter, 5-([4,6-dichlorotriazin-2-yl]amino)fluorescein hydrochloride (DTAF)-dye labeled NFC was used for printing

and crosslinking. According to SEM, on the surface, a rather smooth morphology and compact structure was observed (b). In cross-section (c), in addition to the compact structure, the alignment of the fibers in the printing direction can be seen. This was further confirmed by florescence results, which was obtained from a single strand printed in the longitudinal direction (e) and in a grid pattern (f). The continuous alignment of the DTAF-dyed NFC fibers in the crosslinked NFC/Alg structures is clearly visible in both printing directions.

Gladman et al. printed structures with strong anisotropic swelling using a cellulose nanofiber (CNF)/acrylamide hydrogel to create shapes with biomimetic properties and actuators.[19] Similar anisotropic swelling behavior was observed for our crosslinked samples, which can be attributed to a stabilization effect of the oriented stiff nanofibers. In the longitudinal direction along the printing direction, i.e., the direction of fiber orientation, the samples swelled 153 ± 20% less than perpendicular to the printing direction for the samples crosslinked with Gdl in water alone (no EtOH). The same effect was also observed in 50 wt% EtOH solution, with 121 ± 21% less shrinkage due to fiber orientation. This strong swelling anisotropic effect, referred to in the literature as 4D printing, along with mechanical anisotropy enables the printing of flexible actuators and other biomimetic shapes.[4,53] The same crosslinked samples in the dry state (without liquids) as observed by Gladman et al.[19] for CNF/acrylamide hydrogel showed slight bending (i.e., anisotropy, see Figure S7, Supporting Information), which was due to the presence of some residual stress. However, after the samples were stored in aqueous solutions without ethanol, they regained their previous shape or relaxed again. For specimens used immediately after crosslinking, residual stress was not a problem, as they could be easily inserted into the tensile testing machine after being punched into the dogbone structure.

#### 2.3.2. Effect of Crosslinking Agent

In addition to the impact of fiber alignment, we also investigated the influence of two different crosslinking acids on the mechanical properties of printed structures (with longitudinal fiber orientation, see Figure 1). Crosslinking was done using an excess of 2 M equivalents of the corresponding protons in EtOH/$H_2O$. **Figure 4**a,d shows the comparison of the stress–strain curves and mechanical properties of 3D-printed specimens crosslinked with strong (HCl) and weak acids (condition ii). For comparison, also $CaCl_2$, crosslinked 3D-printed specimen is shown. The specimen crosslinked with Gdl showed a higher tensile strength (6.1 ± 0.3 MPa) compared to two other crosslinked samples with either strong acid HCl (4.8 ± 0.4 MPa) acid or $CaCl_2$ (3.7 ± 0.4 MPa). While the Gdl crosslinked specimen exhibited a tensile modulus of 23.4 ± 1.1 MPa, a 40% lower tensile modulus (14.8 ± 0.9 MPa) was observed for HCl and $CaCl_2$ crosslinked systems. This suggests that the slower and uniform in situ crosslinking induced by Gdl stabilizes the NFC/Alg network in the structure, improving the mechanical properties compared to the other two crosslinkers. Other factors such as increased swelling and pore formation in the case of HCl and structural shrinkage are assumed to play a role in the structural stabilization.

#### 2.3.3. Effect of Sample Storage Media

Not only does the type of crosslinking agent or fiber alignment influence the mechanical properties of the printed samples, but also the medium in which the crosslinked samples can be stored. In this case, the influence of four different storage media (condition iii: EtOH/$H_2O$, NaCl, EtOH/$H_2O$/100 °C, and $H_2O$, see Figure 4b,e) on the mechanical properties of the crosslinked specimens (with longitudinal fiber orientation, see Figure 1) was investigated. For this purpose, the specimen crosslinked using Gdl in EtOH/$H_2O$ medium were studied, which showed better mechanical properties and shape fidelity. In most cases, the sample storage environment and medium are determined by the intended application. The crosslinked samples stored in EtOH/$H_2O$ (the medium used for crosslinking) for 24 h at ambient condition showed no reduction of mechanical properties. The same sample stored in EtOH/$H_2O$ heated to 100 °C for 15 min, to mimic thermal sterilization, showed a 17% and 27% reduction in tensile stress (5.1 ± 0.6 MPa) and tensile modulus (17.1 ± 3 MPa), respectively. Tensile properties were significantly reduced when the crosslinked samples stored in water (pH 7.4). The biomedical applications usually involve aquatic conditions with osmotic pressure originating from various salts. This was simulated by storing the samples in an isotonic 0.9 w% NaCl (physiological) solution and a widely used cell culture medium (advanced Dulbecco's modified Eagle medium (DMEM)) for 24 h. In 0.9 w% NaCl, tensile properties were significantly reduced like the samples stored in water. Similar tensile properties were measured for samples stored in the advanced DMEM media with a tensile modulus of 2.3 ± 0.17 MPa. A long-term storage experiment with the 0.9 w% NaCl and EtOH/$H_2O$ solutions showed that no further significant decrease in mechanical properties was observed over the 3 weeks period (see Figure S8, Supporting Information). Interestingly, in all these cases, the shape fidelity remains unchanged, indicating the high stability of the ionically crosslinked structures in different liquids, including water. This can be seen as a major advantage considering the importance of long-term storage, transport, and handling of samples, especially for biological applications. The benefit of the microbial-free storage option was also investigated by storing the crosslinked samples in water and EtOH/$H_2O$ solutions for up to 6 weeks at ambient conditions. While no microbial growth was observed for the sample stored in EtOH/$H_2O$ solution, more than half of the scaffold was covered with microorganisms under the storage conditions in water and 0.9 w% NaCl (see Figure S9, Supporting Information). This indicates that the EtOH/$H_2O$ medium is the best storage and sterilization medium for long-term preservation of NFC/Alg-based polysaccharide samples.

#### 2.3.4. Effect of $CaCO_3$ Concentration

The influence of $CaCO_3$ (0.09 to 3.3 w%) on the mechanical properties of crosslinked samples, which were stored in EtOH/$H_2O$ or 0.9 w% NaCl solution for 24 h, was also analyzed (see Figure 4c,f). Regardless of the storage medium, the maximum tensile stress was increased with increasing $CaCO_3$ concentration up to about 2.0 to 2.5 w%. After that, a saturation effect was

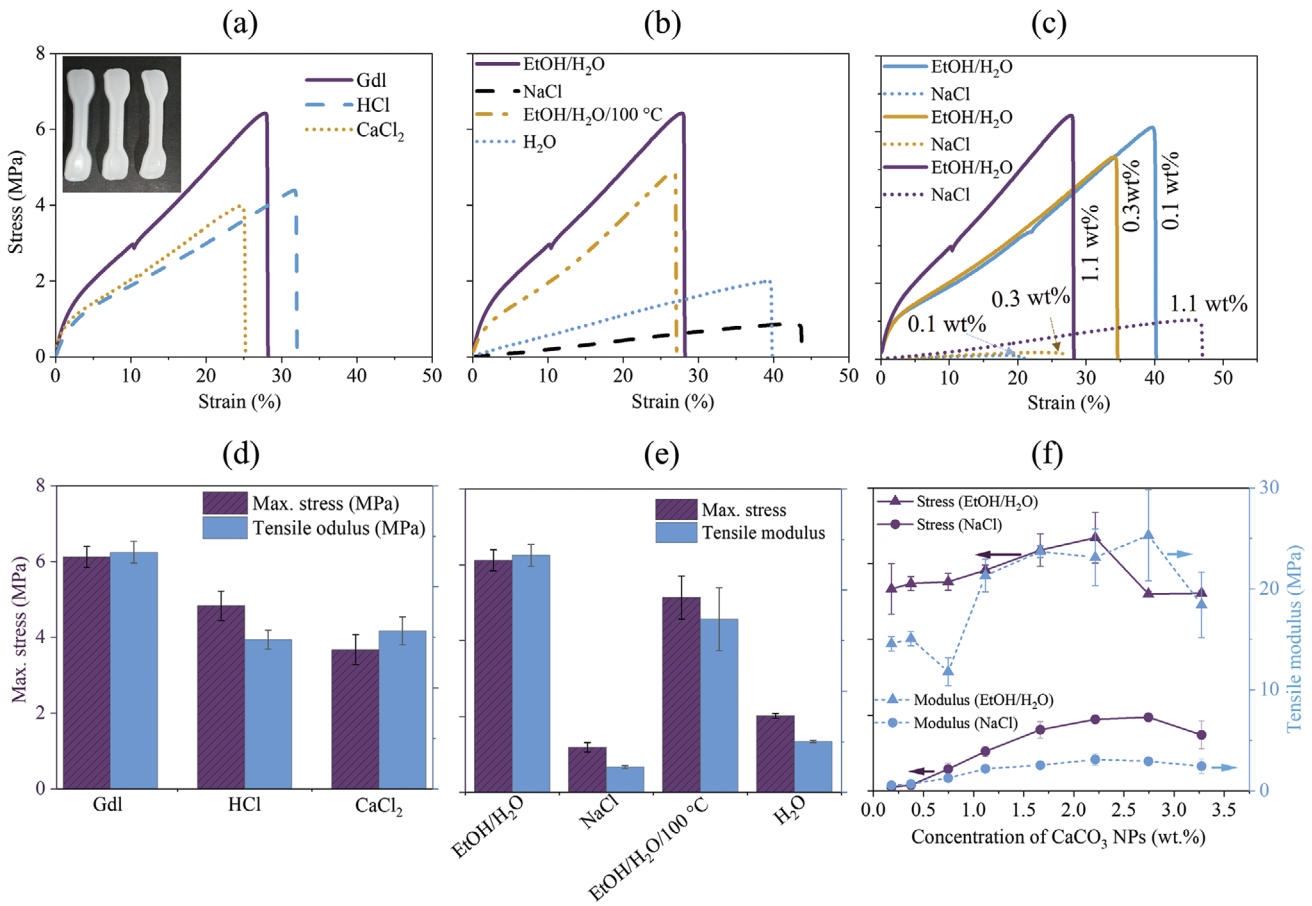


**Figure 4.** Mechanical properties of the NFC/Alg structures crosslinked and stored at different conditions. a,e) Structures (longitudinal) printed from Ink**1.1** and crosslinked using Gdl, HCl, and $CaCl_2$, b,f) structures (longitudinal) printed from Ink**1.1** and crosslinked using Gdl and stored in different conditions, c,f) structures (longitudinal) printed from Ink containing different $CaCO_3$ concentration, crosslinked using Gdl and stored in different $EtOH/H_2O$ and NaCl solution for 24 h.

observed and the maximum stress decreased, possibly due to the increasing formation of defects or voids introduced by $CO_2$ bubbles and insufficient time for the full release conversion of the increased $CaCO_3$ in the structure. By varying the amount of $CaCO_3$, the maximum stress could be controlled in a range from 0.10 ± 0.01 to 1.94 ± 0.11 MPa (19-fold) in 0.9 wt% NaCl and 5.07 ± 0.52 to 6.99 ± 0.32 MPa in $EtOH/H_2O$. The trend of tensile modulus was comparable to tensile stress for the samples stored in both media. For example, the samples stored in $EtOH/H_2O$, the maximum tensile modulus increased with increasing $CaCO_3$ NPs concentration from 14.6 ± 0.7 to 28.4 ± 1.6 MPa. In the same way, for specimen stored in a 0.9 w% NaCl solution, tensile moduli increased from 0.54 ± 0.03 to 3.1 ± 0.6 MPa as the concentration of $CaCO_3$ NPs increased in the structure. This wide range of tensile properties of Gdl crosslinked samples resulting from different $CaCO_3$ allows for several interesting applications. By using different inks with different $CaCO_3$ concentrations, e.g., in printers using dual or even triple extrusion, areas with different mechanical properties could be created and crosslinked in one step. This enables the production of highly anisotropic 3D-printed objects with potential applications in soft robotics or biomedicine (see Section 2.5).

We also compared the mechanical properties of our samples with data from the literature. As can be seen in Table S1 in the Supporting Information, the crosslinked NFC/Alg nanocomposite structures prepared here showed promising tensile properties, even in the wet state, like materials crosslinked with either Gdl or $CaCl_2$ in water. Similarly, our materials outperformed the mechanical properties of several types of natural and synthetic biomaterials (see Table S2, Supporting Information) in wet or dry conditions, which are used for various biomedical (skin,[54–60] cartilage,[61–67] intestine,[25,66] cardiovascular,[68–71] etc.) and nonmedical (e.g., soft robotics[72–74]) applications.

### 2.4. Calcium Ion Leaching

Since mechanical properties can be tailored by the amount of $Ca^{2+}$ supplied during hydrolysis of $CaCO_3$, studying the leaching of $Ca^{2+}$ ions from the scaffold during crosslinking and storage is of interest for deeper understanding and material design. Therefore, we determined the amount of calcium leached into the storage medium ($EtOH/H_2O$ and 0.9 wt%

NaCl), and the remaining calcium in the scaffold by volumetric titration (see the Supporting Information). For this purpose, we used scaffolds containing two different concentrations of $CaCO_3$ NPs (low: 1.1 wt%; high: 3.3 wt%) and crosslinked using Gdl in $EtOH/H_2O$ medium. Results showed that 94 ± 2% of the original amount of calcium remained in the scaffold (**Figure 5**), while the rest was leached in $EtOH/H_2O$. When stored in the physiological solution (0.9 wt% NaCl), 29 ± 1% of the calcium was leached out, possibly to some extent by ion exchange with $Na^+$.[75] The same amount of calcium leaching (with 30.9 ± 1.4%) was observed after 2 weeks of storage in the physiological solution. For the scaffold with a higher amount of $CaCO_3$ (3.3 wt%), more calcium leaching was measured in both $EtOH/H_2O$ (13 ± 1%) and physiological solution (41 ± 2%). It is assumed that saturation occurred, and more alginate and NFC carboxyl groups are fully ionically crosslinked and excess calcium $Ca^{2+}$ ions cannot be retained in the structure. Considering the values obtained from charge titration of Alg (2.63 ± 0.12 mmol $g^{-1}$) and NFC (0.35 ± 0.05 mmol $g^{-1}$),[11,27] only 0.41 wt% $CaCO_3$ is required to form the egg-box structures via ionic crosslinking, with four carboxyl groups coordinated per $Ca^{2+}$ ion (Figure 5).[14,33,34,36]

### 2.5. Possible Applications

The ability to customize the properties of 3D-printed NFC/Alg/$CaCO_3$ nanocomposite at different levels such as concentration of $CaCO_3$, storage medium, or fiber orientation, enables diverse applications. By developing inks with varying $CaCO_3$ concentrations, e.g., in printers using dual or even triple extrusion, areas with different mechanical properties could be created in the same object and crosslinked in one-step. This enables the production of highly anisotropic 3D-printed objects with potential applications in soft robotics[72–74] or biomedicine.[4] To demonstrate the feasibility, we printed a flat sheet (120 × 15 × 2 mm) with three different zones (40 × 15 mm, see **Figure 6**a-i) using inks containing three different $CaCO_3$ concentrations (see Table 1). This was done through a triple extrusion 3D-printing system and the layers were printed longitudinally. The printed structures were crosslinked with Gdl in $EtOH/H_2O$, as was a control sample printed with the same three types of inks but crosslinked with $CaCl_2$. After the crosslinked objects were twisted along their main axis, the twist angles and structural anisotropy were nicely observed. While the structures crosslinked with $CaCl_2$ appeared to exhibit an isotropic behavior with a twist angle of ≈180° for all three zones, those crosslinked with Gdl showed a visible anisotropic effect with twist angles of 90° (Ink**0.1**), 180° (Ink**0.3**), and 270° (Ink**1.1**). Moreover, no destructive $Ca^{2+}$ leaching to other segments was observed, which could lower the anisotropic effect.

The same anisotropic effect could be generated by using the shear force alignment from the DIW printing of the NFC/Alg/$CaCO_3$. In this case, flat sheet with three different zones or segments was also printed and crosslinked. Ink**1.1** was used throughout all segments, but the structures were printed with different printing directions (see Figure 6a-ii). The first zone was printed perpendicular to the main axis (resulting in a perpendicular fiber alignment), the second was printed with a grid alignment by alternating the printing direction (90°) at each layer, and the final zone was printed along the main axis to obtain a longitudinal fiber alignment. By twisting the object along its main axis, the first segment with perpendicular fiber orientation showed the most resistance with a twist angle of ≈90°. The middle segment twisted ≈180° and the segment with the fibers pointing toward the twist axis showed the least resistance at ≈270°. This shows that only by changing the printing path can a similar anisotropic mechanical response be obtained as by triple extrusion of different inks. Moreover, the two effects can be combined by controlling the print path during multiple extrusion printing. Surprisingly, these three crosslinked zones were tightly held together and did not detach during the twisting experiments. When we tested these specimens with tensile testing device, the breaking point was observed in the middle of the sheet and not at the interface of the different zones (see Figure S10, Supporting Information). This implies that the interaction at the edges of the zones is stronger due

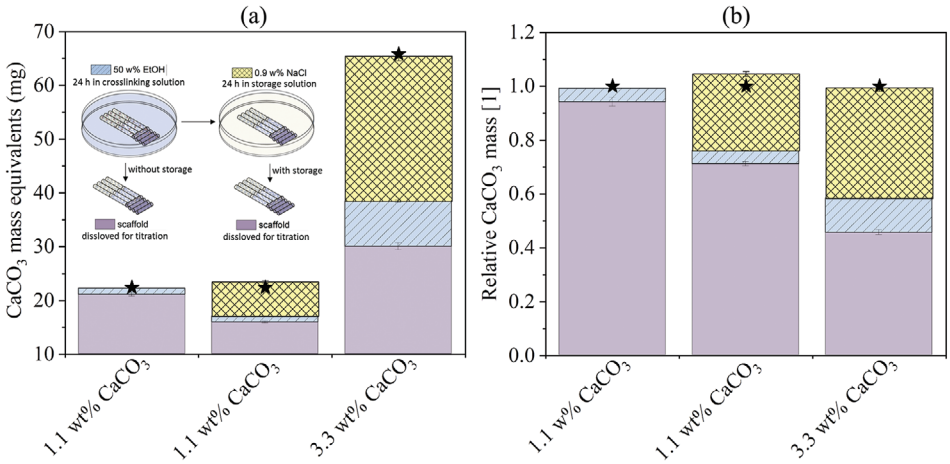


**Figure 5.** The amount of calcium leached (a: in mass equivalent, b: in relative mass) upon storage of the crosslinked samples in $EtOH/H_2O$ and in 0.9 wt% NaCl for 24 h.

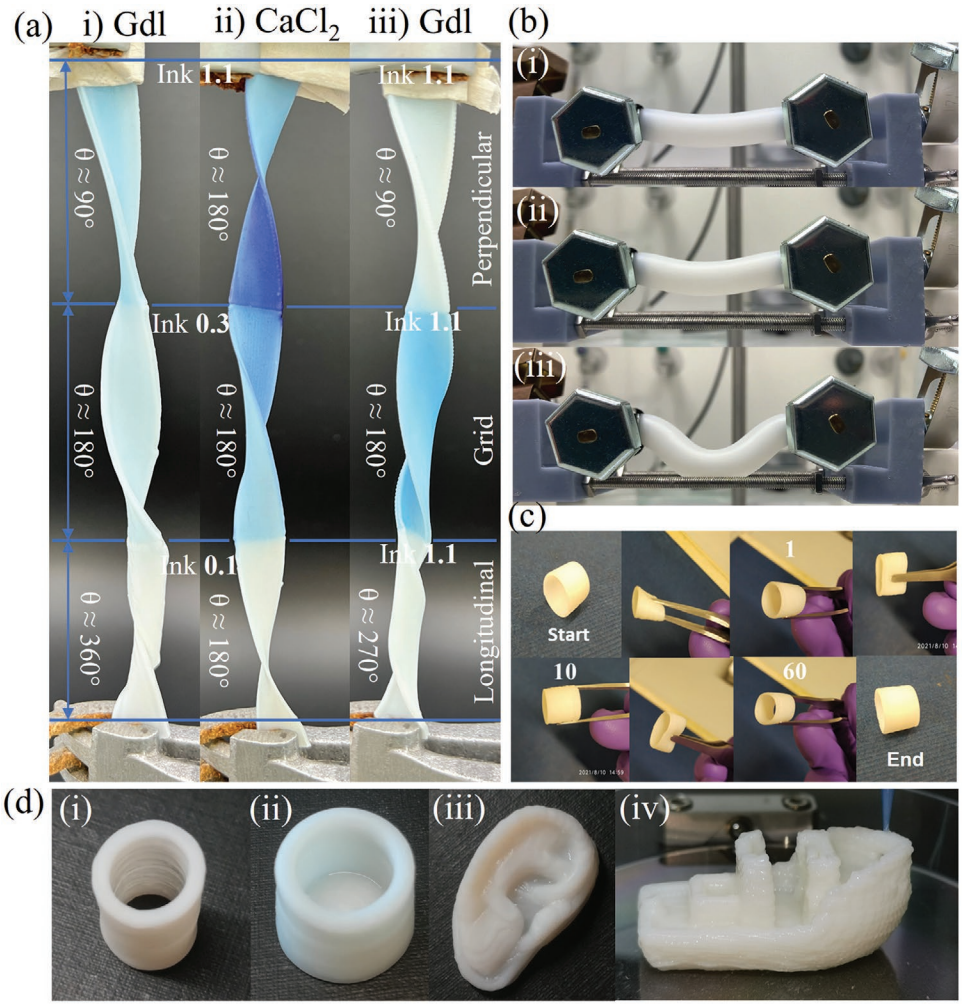


**Figure 6.** Examples of printed and crosslinked structures EtOH/$H_2O$ for different applications. a) 3D-printed and crosslinked NFC/Alg/$CaCO_3$ NPs flat and twisted sheets at different angles: (i: print direction—longitudinal; crosslinking—induced with Gdl, ii: print direction—longitudinal; crosslinking induced with $CaCl_2$, iii: print direction—longitudinal, grid and perpendicular), b) stability test of 3D-printed and Gdl-crosslinked tube (pint direction: longitudinal, dimension: *d*: 8 mm, *h*: 65 mm, wall thickness: 1–1.5 mm) with a pressure up to 160–600 mmHg in the physiological environment up to 24 h (i: 75 mmHg, ii: 300 mmHg, iii: 600 mmHg), c) 3D-printed and Gdl-crosslinked tube (print direction: longitudinal, dimension:) compressed with tweezer and released over a period of 60 times, d) 3D-printed and $CaCO_3$ NPs/Gdl-crosslinked models (print direction: longitudinal) of i) tube, ii) bucket, iii) ear, and iv) boat.

to crosslinking or interfacial adhesion between structurally similar NFC and Alg.[27,76]

The NFC-Alg-based scaffolds have been used in TE as load-bearing structures such as cartilage or bone, which typically require a modulus of elasticity greater than 1 MPa and a water content greater than 60%.[36] The material presented in this study achieves a tensile modulus of 2–3 MPa, elongation at break of more than 50%, and water content of about 90% under physiological conditions (0.9 wt% NaCl). Therefore, our fully bio-based material could be an attractive candidate for biomedical applications with challenging mechanics, ranging from cartilage (e.g., ear) to cardiovascular applications (e.g., aorta). To create a simplified model of a vascular system, a tube with an inner diameter of 8 mm, a height of 65 mm, and a wall thickness of 1–1.5 mm was 3D printed (with radial fiber orientation) and crosslinked (see Figure 6b-i–iii). By applying a hydrostatic pressure of 160 mmHg using a 0.9 w% NaCl solution, pressure stability was tested over 24 h. Results showed an increase of diameter up to 0.5 mm and no visible droplet formation or leakage from the tubing. Even at a pressure higher than the physiological conditions of 600 mmHg, the tube did not rupture but showed a pronounced linear expansion. While the tube length increased by 29% between the calottes, the radii showed less expansion at 9% between 0 and 600 mmHg. One possible explanation is that the radial alignment of the fibers, originating from the circumferential printing path, restricts the expansion of the diameter. This stabilization by the radially aligned fibers allowed high fracture pressures of up to 3.4 bar. It was expected that the hydrophilic and charged components such as NFC and Alg of the tubular structure would swell during the experiments with hydrostatic pressure and the structure would collapse. Surprisingly, no such behavior was

 

observed, indicating that the structure is highly (fluid) water resistant. Such water-proof or fluid resistance is rarely or never reported for purely hydrophilic composites, especially for ionically crosslinked NFC/Alg nanocomposites. These special properties could be particularly advantageous for hydrophilic biobased materials in blood-related applications.

The applicability of the NFC/Alg-based inks was further demonstrated by creating flexible tube (length: 10 mm, wall thickness: 1.5 mm, Figure 6c). After repeated squeezing with tweezers and releasing up to 60 times, the tube regained its original dimension and shape fidelity, demonstrating its shape-recovery, which might have some potential use in cardiovascular-related TE applications. The flexibility of our optimized DIW ink was also illustrated by printing even more complex structures. With nozzle diameters of 0.26 and 0.41 mm, pressures between 140 and 160 kPa and printing speeds up to 25 mm $s^{-1}$, a tube, an ear model, a bucket, and the "3Dbenchy" model without a roof were printed with high shape fidelity (see Figure 6d-i–iv). Overall, it can be stated that 3D objects of functional NFC/Alg nanocomposites with structural, mechanical, and swelling anisotropy can be created by the proper combination of inks, crosslinking chemistry, and DIW-assisted shear-induced alignment for the desired anisotropic functional performances.

To investigate possible adverse effects of the crosslinked samples on cell viability, an indirect biocompatibility or cytotoxicity assay was performed similar to the standard ISO 10993-5:2009(E).[27,34,77] For this purpose, we used 3D-printed and Gdl-crosslinked objects of Ink**1.1** because they exhibited better mechanical and storage stability (Figures 3 and 4). Polylactide (PLA) was chosen as a control because it has been shown to be biocompatible in previous studies.[78,79] The results (see **Figure 7**) showed that the NFC/Alg samples were compatible with the tested cells (HEK-293).

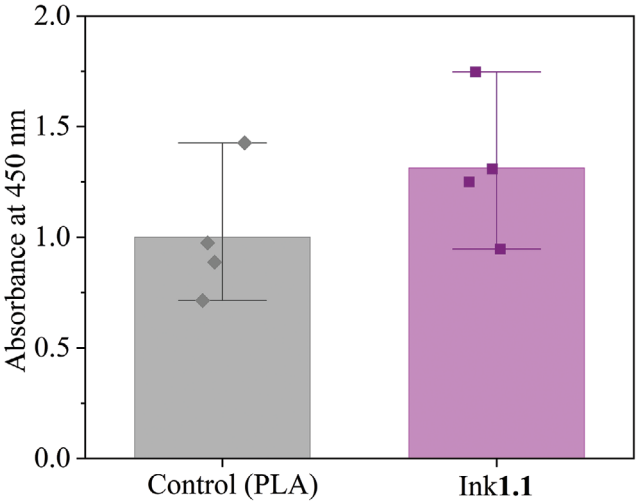


**Figure 7.** Viability of HEK-293 cells on sample extracts (supernatants) of 3D-printed PLA (control) and Gdl-crosslinked NFC/Alg (Ink**1.1**) structures. Experiments were performed for 24 h. The values were normalized to the absorbance of PLA.

## 3. Conclusions

We developed advanced materials from functional polysaccharide nanocomposites exhibiting structural, swelling, and mechanical anisotropy. Such anistropic materials with high wet strength, pressure, and fluid resistance were created using the combination of homogenous inks, DIW shear-induced alignment, crosslinking chemistry, and medium. A new homogenous ink system based on NFC, Alg, and $CaCO_3$ for DIW 3D printing with shear thinning properties and printability was developed. All inks showed higher viscosity and modulus (storage and loss) compared to the individual components of the ink. This resulted in excellent ink extrudability and printed structures in various 3D forms (sheets, tubes, buckets, ears, and boat) with high shape fidelity. Increasing the concentration of $CaCO_3$ NPs did not significantly improve the rheological behavior of the ink. Compared to $CaCl_2$, HCl, the in situ crosslinking induced by Gdl showed no structural collapse resulted in structures with highest shape fidelity and less swelling. This is even more pounced when the crosslinking was performed in $EtOH/H_2O$ crosslinking medium. The mechanical properties of the structures, measured in the wet state, are highly tunable, depending on the conditions used. Crosslinking with the $CaCO_3$ NPs/Gdl system showed the highest tensile properties compared to other crosslinking agents. Increase of $CaCO_3$ NPs in the printed structure increased the tensile properties and stability after crosslinking. In general, the structures printed in the longitudinal direction demonstrated the maximum tensile strength and modulus. A significant decrease in tensile properties was observed when the samples were stored in physiological medium compared to other storage medium. This was related to the release of bound calcium over time. Surprisingly, no significant reduction in tensile properties was noticed for the crosslinked structures that were boiled or sterilized at higher temperature. The application of the developed ink and crosslinking method was demonstrated by printing twistable yet stable structures with three different segments differing in composition and fiber orientation or printing direction. This approach was further extended to print a tubular structure, a modular system for vascular or aortic tissue capable of withstanding pressures up to 600 mmHg in the phytological environment. Given the nature of inks and crosslinked structures with tunable properties and biocompatibility, the proposed system has high potential for mimicking biological properties and developing complex tissue prototypes in soft robotics.

## 4. Experimental Section

*Materials*: NFC suspension (3 wt% solid content) was purchased from the University of Maine, USA (charge 0.35 ± 0.05 mmol $g^{-1}$). Sodium salt of alginic acid from brown algae (COONa: 2.63 ± 0.12 mmol $g^{-1}$), glucono-$\delta$-lactone (GdL, ≥99 %), ethylenediaminetetraacetic acid disodium salt dihydrate ($Na_2EDTA*2H_2O$, ≥99 %), calcium chloride ($CaCl_2$, 99%), DTAF (≥90 %) and calconcarboxylic acid were purchased from Sigma-Aldrich, Austria. Calcium carbonate nanoparticles ($CaCO_3$ NPs, 99.5%) were purchased from Solvay Chemicals International, Belgium. Ethanol (≥99 %) was purchased from VWR Chemicals,Austria. Hydrochloric acid (HCl, 37 w%) and sodium hydroxide (NaOH, ≥98 %) and advanced DMEM/F12 media were purchased from Fisher Scientific, Austria.

SmoothFlow tapered tips (250, 410 µm), syringe barrel pistons, and fluid dispensing polyethylene-based plastic cartridges were purchased from Nordson, UK. ECO Resin (black, gray, and transparent) was purchased from Anycubic, China. NicePVA and ecoPLA-filament were purchased from 3DJake, Austria.

*Preparation of Nanocomposite Inks for DIW*: The following general procedure was used to prepare the inks with varying compositions for the DIW (see Table 1). Briefly, 20 g of NFC (3.0 w%) was taken in a 50 mL falcon tube. To this, the appropriate amounts of $CaCO_3$ NP were suspended followed by mixing at 2000 rpm for 60 s using a mechanical laboratory stirrer RZR 2005(Heidolph, Germany). The latter was equipped with an in-house 3D-printed stirrer (see Figures S2d and S3d, right side, Supporting Information). Following this, 1.33 g of Alg was added and then mixed at 2000 rpm for 10 min. This resulted in a slightly homogenous ink, which was subsequently stored in a refrigerator at 2–8 °C or directly used for printing.

*Rheology*: The rheological properties of inks with different $CaCO_3$ NPs concentrations (1.67, 0.34, and 0.17 w%) were evaluated with a modular compact rheometer MCR 502 ( Anton Paar, Austria). Viscosity curves were measured from a shear rate between 0.1 and 100 $s^{-1}$. Amplitude sweeps were measured at shear deformations between 0.001 and 1.

*DIW 3D Printing*: To generate 3D models, the open-source program FreeCAD 0.19 or 3D Builder 18.0.1931.0 (Microsoft Corporation) was used (dimensions are given in Table S2, Supporting Information). Using the inks mentioned in Table 1, different shapes were 3D printed. Circular or square-shaped scaffolds (radius 7–20 mm; height: 0.2–8 cm, number of corners: 100) and cubic shape scaffolds (diameter 25 mm, height 3.5 mm, number of corners: 4) were built in a layer-by-layer fashion. These dimensions were created by using GeSiM Robotics BioScaffolder 3.2 software (GeSim, Germany). To create more complex 3D-printed structures, the. stl or .3MF files were integrated and processed by the GeSim Robotics BS 3.2 software. The composite inks were extruded from a 30 mL polyethylene-based plastic barrel (Nordson, UK) equipped with tapered tips (Nordson, UK Limited) with an inner diameter of 410 µm onto polystyrene petri dishes. The scaffolds were printed with extrusion pressures between 130 and 160 kPa, print speeds of 25 mm $s^{-1}$, a strand distance of 0.50 mm, and a strand height and width of 0.44 mm. All structures were printed in three different patterns to control the fiber orientation within the final object. This was done by rotating 90° of each subsequent layer or kept constant for the whole print. All freshly printed specimens were subsequently crosslinked as mentioned in the section below.

*Ionic Crosslinking*: Two different crosslinking methods were used. In method 1, the printed scaffolds were immersed into a solution of ethanol/water (50/50 wt%) or water together with either Gdl or HCl as acid (4.00 M equiv. regarding $CaCO_3$) for 24 h under ambient conditions. The mass ratio of scaffold to solution (water/ethanol or water) was 1 to 10. During crosslinking time, the samples were gently shaken with a Unimax 2010 (Heidolf, Germany). In method 2, the crosslinking was performed in the same way as mentioned before using $CaCl_2$ (1.00 M equiv. in regard of $CaCO_3$) dissolved in water/ethanol solution (50/50 wt%) for 24 h. In this case, $CaCO_3$ remained intact.

*$CO_2$ Release Kinetics Measurements*: A self-designed and 3D-printed measurement cell equipped with a precalibrated SCD30 $CO_2$-sensor (Sensioron, Switzerland) controlled with an ESP32 development board (see Figure S2, Supporting Information) was used for monitoring the amount of $CO_2$ from $CaCO_3$ during crosslinking. The temperature in the cell was controlled between 24.0 and 26.0 °C using a thermostat (Julabo F12, Germany) together with copper coils in the cell. For this measurement, the samples were printed using the Ink**1.1** in cylindrical form with different radius (6 and 10 mm) and height (6 and 2.2 mm) but approximately the same volume. The printed samples were placed in the measurement cell followed by the addition of crosslinking solutions (see above section for the type of crossing solution). The concentration of released $CO_2$ was monitored until equilibrium or for the period of 24 h.

*Attenuated Total Reflectance-Infrared Spectroscopy*: IR spectra were measured using ALPHA-P (Bruker, USA) spectrometer. Scan range was set from 4000 to 375 $cm^{-1}$, with a total of 40 scans performed at a resolution of 4 $cm^{-1}$. For this analysis, the crosslinked samples were air dried and used.

*SEM*: The morphology of air-dried samples was analyzed by field-emission (FE)-SEM. A Carl Zeiss FE-SEM SUPRA 35 VP electron microscope was used. The images were recorded with an acceleration voltage of 1 kV. The chemical compositions of samples were examined using an EDX detector (model OXFORD INCA 200, Oxford Instruments, Germany). The EDX detector is equipped with a liquid nitrogen cooled X-ray detector (Si(Li)—silicon with lithium) having 10 $mm^2$ crystal area. The working distance for the EDX detector was 8.5 mm and the electron energy (acceleration voltage) was 10 keV. The samples were mounted on sample holders and no sputtering on the sample surfaces was performed. For the elemental mapping, a 10 nm gold layer was sputtered on the sample surface.

*Mechanical Tests*: For the tensile tests, dog bone specimens (thickness: 1.00–2.50 mm) were punched out from 50 mm × 8.5 mm 3D-printed specimen according to DIN 53504 S3A. The tensile tests were carried out using Shimanzu AGS-X (Japan) universal mechanical testing machine with a speed of 50 mm $min^{-1}$ and standard clamps. At least four specimens were tested for each condition.

*In Vitro Biocompatibility Analysis*: For the biocompatibility test, 3D-printed circular disks (diameter: 22 mm; height: 2.0 mm) from polylactic acid (PLA) as control and from the Ink**1.1** crosslinked with Gdl in $EtOH/H_2O$ were used. PLA disks were printed using a Ender 3 V2 (Creality, China) FDM printer at 200 °C nozzle temperature and at 50 mm $s^{-1}$ printing speed. The Gdl-crosslinked Ink**1.1** disks were stored in a storage solution ($1.05 \times 10^{-3}$ M $CaCl_2$, $0.7 \times 10^{-3}$ M $MgCl_2$, and $150 \times 10^{-3}$ M NaCl) for 24 h. This procedure was repeated four times to minimize swelling. Afterward, the samples in the storage solution were autoclaved for 15 min at 125 °C. PLA disks were sterilized using 70 wt% EtOH prior to cell testing.

Prior to the cell testing, the disks (PLA and Ink**1.1**) were incubated with the DMEM F12 cell culture medium for 24 h. Afterward, the supernatants were collected and tested on HEK-293 cells (human embryonic kidney cells) for 24 h to access their biocompatibility/viability. The viability of these cells was assessed using a cell counting kit 8 (CCK-8) according to the manufacturer's instructions (Dojindo Molecular Technologies, Inc.). Briefly, cells (3000 cells per well) were incubated in 96-well plates for 24 h with the supernatant either from the PLA or Ink**1.1**. Subsequently, 10 µL of CCK-8 per 100 µL of culture medium was added to each well, and the cells were incubated for 3 h at 37 °C. Cell viability was assessed as absorbance of each well at 450 nm measured by a microplate reader. The absorbance values were normalized to PLA, chosen as a control. All experiments were performed in quadruplicate.

## Supporting Information

Supporting Information is available from the Wiley Online Library or from the author.

## Acknowledgements

The authors thank Dr. Matej Bračič from University of Maribor/Slovenia for performing polyelectrolyte charge titration experiments.

## Conflict of Interest

The authors declare no conflict of interest.

## Data Availability Statement

The data that support the findings of this study are available in the supplementary material of this article.

## Keywords

3D printing, anisotropy nanocomposites, biomedical applications, mechanical properties, nanocellulose alginate

Received: October 10, 2022
Revised: December 23, 2022
Published online: February 3, 2023

[1] C. Sanchez, H. Arribart, M. M. Giraud Guille, *Nat. Mater.* **2005**, *4*, 277.
[2] A. R. Studart, *Chem. Soc. Rev.* **2016**, *45*, 359.
[3] H. Abe, K. Hayashi, M. Sato, *Data Book on Mechanical Properties of Living Cells, Tissues and Organs*, Springer Tokyo, Tokyo **1996**.
[4] J. Chen, X. Liu, Y. Tian, W. Zhu, C. Yan, Y. Shi, L. B. Kong, H. J. Qi, K. Zhou, *Adv. Mater.* **2022**, *34*, 2102877.
[5] A. R. Studart, *Adv. Funct. Mater.* **2013**, *23*, 4423.
[6] M. Vatankhah-Varnosfaderani, W. F. M. Daniel, M. H. Everhart, A. A. Pandya, H. Liang, K. Matyjaszewski, A. V. Dobrynin, S. S. Sheiko, *Nature* **2017**, *549*, 497.
[7] Y. C. Fung, *Am. Zool.* **2015**, *24*, 13.
[8] G. Singh, A. Chanda, *Biomed. Mater.* **2021**, *16*, 062004.
[9] C. F. Guimarães, L. Gasperini, A. P. Marques, R. L. Reis, *Nat. Rev. Mater.* **2020**, *5*, 351.
[10] T. Mohan, T. Maver, A. D. Štiglic, K. Stana-Kleinschek, R. Kargl, in *Fundamental Biomaterials: Polymers* (Eds: S. Thomas, P. Balakrishnan, M. S. Sreekala), Woodhead Publishing, Sawston, Cambridge **2018**, pp. 105–141.
[11] A. D. Štiglic, F. Gürer, F. Lackner, D. Bračič, A. Winter, L. Gradišnik, D. Makuc, R. Kargl, I. Duarte, J. Plavec, U. Maver, M. Beaumont, K. S. Kleinschek, T. Mohan, *iScience* **2022**, *25*, 104263.
[12] R. L. Mauck, B. M. Baker, N. L. Nerurkar, J. A. Burdick, W.-J. Li, R. S. Tuan, D. M. Elliott, *Tissue Eng., Part B* **2009**, *15*, 171.
[13] K. Wang, C.-C. Ho, C. Zhang, B. Wang, *Engineering* **2017**, *3*, 653.
[14] G. Janarthanan, S. Lee, I. Noh, *Adv. Funct. Mater.* **2021**, *31*, 2104441.
[15] G. Siqueira, D. Kokkinis, R. Libanori, M. K. Hausmann, A. S. Gladman, A. Neels, P. Tingaut, T. Zimmermann, J. A. Lewis, A. R. Studart, *Adv. Funct. Mater.* **2017**, *27*, 1604619.
[16] L. Berglund, T. Nissilä, D. Sivaraman, S. Komulainen, V.-V. Telkki, K. Oksman, *ACS Appl. Mater. Interfaces* **2021**, *13*, 34899.
[17] D. Kokkinis, M. Schaffner, A. R. Studart, *Nat. Commun.* **2015**, *6*, 8643.
[18] D. Chimene, R. Kaunas, A. K. Gaharwar, *Adv. Mater.* **2020**, *32*, 1902026.
[19] A. S. Gladman, E. A. Matsumoto, R. G. Nuzzo, L. Mahadevan, J. A. Lewis, *Nat. Mater.* **2016**, *15*, 413.
[20] P. Siqueira, É. Siqueira, A. E. d. Lima, G. Siqueira, A. D. Pinzón-Garcia, A. P. Lopes, M. E. C. Segura, A. Isaac, F. V. Pereira, V. R. Botaro, *Nanomaterials* **2019**, *9*, 78.
[21] R. Kaufmann, C. J. Zech, M. Takes, P. Brantner, F. Thieringer, M. Deutschmann, K. Hergan, B. Scharinger, S. Hecht, R. Rezar, B. Wernly, M. Meissnitzer, *J. Digital Imaging* **2022**, *35*, 9.
[22] D. Zhalmuratova, T.-G. La, K. T.-T. Yu, A. R. A. Szojka, S. H. J. Andrews, A. B. Adesida, C.-I. Kim, D. S. Nobes, D. H. Freed, H.-J. Chung, *ACS Appl. Mater. Interfaces* **2019**, *11*, 33323.
[23] S. Caillol, *Molecules* **2021**, *26*, 112.
[24] T. J. Hinton, Q. Jallerat, R. N. Palchesko, J. H. Park, M. S. Grodzicki, H.-J. Shue, M. H. Ramadan, A. R. Hudson, A. W. Feinberg, *Sci. Adv.* **2015**, *1*, e1500758.
[25] S. Malladi, D. Miranda-Nieves, L. Leng, S. J. Grainger, C. Tarabanis, A. P. Nesmith, R. Kosaraju, C. A. Haller, K. K. Parker, E. L. Chaikof, A. Günther, *ACS Biomater. Sci. Eng.* **2020**, *6*, 4236.
[26] K. Li, C. M. Clarkson, L. Wang, Y. Liu, M. Lamm, Z. Pang, Y. Zhou, J. Qian, M. Tajvidi, D. J. Gardner, H. Tekinalp, L. Hu, T. Li, A. J. Ragauskas, J. P. Youngblood, S. Ozcan, *ACS Nano* **2021**, *15*, 3646.
[27] T. Mohan, A. Dobaj Štiglic, M. Beaumont, J. Konnerth, F. Gürer, D. Makuc, U. Maver, L. Gradišnik, J. Plavec, R. Kargl, K. Stana Kleinschek, *ACS Appl. Bio Mater.* **2020**, *3*, 1197.
[28] X. Yu, H. Zhang, Y. Miao, S. Xiong, Y. Hu, *J. Leather Sci. Eng.* **2022**, *4*, 11.
[29] W. Sun, J. W. Tashman, D. J. Shiwarski, A. W. Feinberg, V. A. Webster-Wood, *ACS Biomater. Sci. Eng.* **2022**, *8*, 303.
[30] M. E. Culica, A.-L. Chibac-Scutaru, T. Mohan, S. Coseri, *Biosens. Bioelectron.* **2021**, *182*, 113170.
[31] H. Rabillé, T. A. Torode, B. Tesson, A. Le Bail, B. Billoud, E. Rolland, S. Le Panse, M. Jam, B. Charrier, *Sci. Rep.* **2019**, *9*, 12956.
[32] D. Nguyen, D. A. Hägg, A. Forsman, J. Ekholm, P. Nimkingratana, C. Brantsing, T. Kalogeropoulos, S. Zaunz, S. Concaro, M. Brittberg, A. Lindahl, P. Gatenholm, A. Enejder, S. Simonsson, *Sci. Rep.* **2017**, *7*, 658.
[33] N. Lin, C. Bruzzese, A. Dufresne, *ACS Appl. Mater. Interfaces* **2012**, *4*, 4948.
[34] K. Markstedt, A. Mantas, I. Tournier, H. Martínez Ávila, D. Hägg, P. Gatenholm, *Biomacromolecules* **2015**, *16*, 1489.
[35] C. C. Piras, D. K. Smith, *J. Mater. Chem. B* **2020**, *8*, 8171.
[36] E. B. Heggset, B. L. Strand, K. W. Sundby, S. Simon, G. Chinga-Carrasco, K. Syverud, *Cellulose* **2019**, *26*, 581.
[37] X. Lan, Z. Ma, A. R. A. Szojka, M. Kunze, A. Mulet-Sierra, M. J. Vyhlidal, Y. Boluk, A. B. Adesida, *Front. Bioeng. Biotechnol.* **2021**, *9*, 766399.
[38] G. Janarthanan, J. H. Kim, I. Kim, C. Lee, E.-J. Chung, I. Noh, *Biofabrication* **2022**, *14*, 035013.
[39] J. Jang, Y.-J. Seol, H. J. Kim, J. Kundu, S. W. Kim, D.-W. Cho, *J. Mech. Behav. Biomed. Mater.* **2014**, *37*, 69.
[40] S. Liu, Y. Hu, J. Zhang, S. Bao, L. Xian, X. Dong, W. Zheng, Y. Li, H. Gao, W. Zhou, *Macromol. Mater. Eng.* **2019**, *304*, 1800698.
[41] L. Sardelli, M. Tunesi, F. Briatico-Vangosa, P. Petrini, *Soft Matter* **2021**, *17*, 8105.
[42] O. Aarstad, E. B. Heggset, I. S. Pedersen, S. H. Bjørnøy, K. Syverud, B. L. Strand, *Polymers* **2017**, *9*, 378.
[43] L. Amornkitbamrung, D. Bračič, M. Bračič, S. Hribernik, J. Malešič, U. Hirn, A. Vesel, K. S. Kleinschek, R. Kargl, T. Mohan, *ACS Omega* **2020**, *5*, 29243.
[44] C. Sun, Y. Gao, Q. Zhong, *Food Hydrocolloids* **2018**, *82*, 173.
[45] S. A. Parke, G. G. Birch, D. B. MacDougall, D. A. Stevens, *Chem. Senses* **1997**, *22*, 53.
[46] D. Mohan, N. F. Khairullah, Y. P. How, M. S. Sajab, H. Kaco, *Polymers* **2020**, *12*, 986.
[47] M. Henriksson, L. A. Berglund, P. Isaksson, T. Lindström, T. Nishino, *Biomacromolecules* **2008**, *9*, 1579.
[48] J. Foroughi, G. M. Spinks, G. G. Wallace, *J. Mater. Chem.* **2011**, *21*, 6421.
[49] F. Ansari, S. Galland, M. Johansson, C. J. G. Plummer, L. A. Berglund, *Composites, Part A* **2014**, *63*, 35.
[50] M. Bordoni, E. Karabulut, V. Kuzmenko, V. Fantini, O. Pansarasa, C. Cereda, P. Gatenholm, *Cells* **2020**, *9*, 682.
[51] M. K. Hausmann, P. A. Rühs, G. Siqueira, J. Läuger, R. Libanori, T. Zimmermann, A. R. Studart, *ACS Nano* **2018**, *12*, 6926.
[52] A. Schwab, C. Hélary, R. G. Richards, M. Alini, D. Eglin, M. D'Este, *Mater. Today Bio* **2020**, *7*, 100058.
[53] H. Arslan, A. Nojoomi, J. Jeon, K. Yum, *Adv. Sci.* **2019**, *6*, 1800703.
[54] Q. Zhou, K. Yang, J. He, H. Yang, X. Zhang, *J. Mater. Chem. C* **2019**, *7*, 14913.
[55] D. E. López Angulo, P. J. do Amaral Sobral, *Int. J. Biol. Macromol.* **2016**, *92*, 645.

[56] S. Chen, L. Sun, X. Zhou, Y. Guo, J. Song, S. Qian, Z. Liu, Q. Guan, E. Meade Jeffries, W. Liu, Y. Wang, C. He, Z. You, *Nat. Commun.* **2020**, *11*, 1107.
[57] T. Wang, J. Wang, R. Wang, P. Yuan, Z. Fan, S. Yang, *New J. Chem.* **2019**, *43*, 8684.
[58] V. Y. Chakrapani, A. Gnanamani, V. R. Giridev, M. Madhusoothanan, G. Sekaran, *J. Appl. Polym. Sci.* **2012**, *125*, 3221.
[59] P. Jiang, C. Yan, Y. Guo, X. Zhang, M. Cai, X. Jia, X. Wang, F. Zhou, *Biomater. Sci.* **2019**, *7*, 1805.
[60] P. Squinca, L. Berglund, K. Hanna, J. Rakar, J. Junker, H. Khalaf, C. S. Farinas, K. Oksman, *Biomacromolecules* **2021**, *22*, 3202.
[61] S. E. Bakarich, M. I. H. Panhuis, S. Beirne, G. G. Wallace, G. M. Spinks, *J. Mater. Chem. B* **2013**, *1*, 4939.
[62] Q. Chen, L. Zhu, C. Zhao, Q. Wang, J. Zheng, *Adv. Mater.* **2013**, *25*, 4171.
[63] J. Wei, J. Wang, S. Su, S. Wang, J. Qiu, Z. Zhang, G. Christopher, F. Ning, W. Cong, *RSC Adv.* **2015**, *5*, 81324.
[64] F. Gao, Z. Xu, Q. Liang, H. Li, L. Peng, M. Wu, X. Zhao, X. Cui, C. Ruan, W. Liu, *Adv. Sci.* **2019**, *6*, 1900867.
[65] F. Gao, Z. Xu, Q. Liang, B. Liu, H. Li, Y. Wu, Y. Zhang, Z. Lin, M. Wu, C. Ruan, W. Liu, *Adv. Funct. Mater.* **2018**, *28*, 1706644.
[66] F. Yang, V. Tadepalli, B. J. Wiley, *ACS Biomater. Sci. Eng.* **2017**, *3*, 863.
[67] Y. Hou, C. A. Schoener, K. R. Regan, D. Munoz-Pinto, M. S. Hahn, M. A. Grunlan, *Biomacromolecules* **2010**, *11*, 648.
[68] B. Xu, Y. Li, X. Fang, G. A. Thouas, W. D. Cook, D. F. Newgreen, Q. Chen, *J. Mech. Behav. Biomed. Mater.* **2013**, *28*, 354.
[69] R. Hernández-Córdova, D. A. Mathew, R. Balint, H. J. Carrillo-Escalante, J. M. Cervantes-Uc, L. A. Hidalgo-Bastida, F. Hernández-Sánchez, *J. Biomed. Mater. Res., Part A* **2016**, *104*, 1912.
[70] M. Castilho, D. Feyen, M. Flandes-Iparraguirre, G. Hochleitner, J. Groll, P. A. F. Doevendans, T. Vermonden, K. Ito, J. P. G. Sluijter, J. Malda, *Adv. Healthcare Mater.* **2017**, *6*, 1700311.
[71] N. Amdursky, M. M. Mazo, M. R. Thomas, E. J. Humphrey, J. L. Puetzer, J.-P. St-Pierre, S. C. Skaalure, R. M. Richardson, C. M. Terracciano, M. M. Stevens, *J. Mater. Chem. B* **2018**, *6*, 5604.
[72] G. Guo, Q. Wu, F. Liu, J. Yin, Z. L. Wu, Q. Zheng, J. Qian, *Adv. Funct. Mater.* **2022**, *32*, 2108548.
[73] S. Y. Zheng, Y. Shen, F. Zhu, J. Yin, J. Qian, J. Fu, Z. L. Wu, Q. Zheng, *Adv. Funct. Mater.* **2018**, *28*, 1803366.
[74] X. Shi, J. Zhang, N. Corrigan, C. Boyer, *Polym. Chem.* **2022**, *13*, 44.
[75] Y. Qin, H. Hu, A. Luo, *J. Appl. Polym. Sci.* **2006**, *101*, 4216.
[76] A. Dobaj Štiglic, R. Kargl, M. Beaumont, C. Strauss, D. Makuc, D. Egger, J. Plavec, O. J. Rojas, K. Stana Kleinschek, T. Mohan, *ACS Biomater. Sci. Eng.* **2021**, *7*, 3618.
[77] M. Milojević, L. Gradišnik, J. Stergar, M. Skelin Klemen, A. Stožer, M. Vesenjak, P. Dobnik Dubrovski, T. Maver, T. Mohan, K. Stana Kleinschek, U. Maver, *Appl. Surf. Sci.* **2019**, *488*, 836.
[78] J. I. Castro, C. H. Valencia Llano, D. L. Tenorio, M. Saavedra, P. Zapata, D. P. Navia-Porras, J. Delgado-Ospina, M. N. Chaur, J. H. M. Hernández, C. D. Grande-Tovar, *Molecules* **2022**, *27*, 3640.
[79] M. C. Wurm, T. Möst, B. Bergauer, D. Rietzel, F. W. Neukam, S. C. Cifuentes, C. v. Wilmowsky, *J. Biol. Eng.* **2017**, *11*, 29.